symmetry

MDPI

Article

The Effects of Reduced Gravity and Radiative Heat Transfer on the Magnetohydrodynamic Flow Past a Non-Rotating Stationary Sphere Surrounded by a Porous Medium

Amir Abbas [1,*], Ioannis E. Sarris [2], Muhammad Ashraf [3], Kaouther Ghachem [4,*], Nidhal Hnaien [5] and Badr M. Alshammari [6]

[1] Department of Mathematics, Faculty of Science, University of Gujrat, Sub-Campus, Mandi Bahauddin 50400, Pakistan
[2] Department of Mechanical Engineering, University of West Attica, 12244 Athens, Greece
[3] Department of Mathematics, Faculty of Science, University of Sargodha, Sargodha 40100, Pakistan
[4] Department of Industrial Engineering and Systems, College of Engineering, Princess Nourah bint Abdulrahman University, P.O. Box 84428, Riyadh 11671, Saudi Arabia
[5] Research Laboratory of Metrology and Energy Systems, National Engineering School, University of Monastir, LR18ES21, Monastir 5000, Tunisia
[6] Department of Electrical Engineering, College of Engineering, University of Ha'il, P.O. Box 2440, Ha'il City 81451, Saudi Arabia
* Correspondence: cfdamirabbas4693@gmail.com (A.A.); kgmaatki@pnu.edu.sa (K.G.)

Abstract: In the present study, the effects of reduced gravity and solar radiation on the magnetohydrodynamics (MHD) fluid flow and heat transfer past a solid and stationary sphere embedded in a porous medium are investigated. A model describing the considered configuration is put in dimensionless form using appropriate dimensionless variables and then transformed to primitive form for a smooth algorithm on a computing tool. A primitive form of the model is solved by employing the finite difference method. Solutions for variables of interest, such as velocity distribution and temperature field, along with their gradients, are depicted in graphs and tables. The main goal of the paper is to study the physical impact of reduced gravity on heat transfer and fluid flow around a sphere surface inserted in a porous medium in the presence of an applied magnetic field and solar radiation. The effects of the governing parameters, which are the reduced gravity parameter, magnetic field parameter, radiation parameter, porous medium parameter, and the Prandtl number, are discussed and physically interpreted. The displayed solutions indicate that velocity rises with the reduced gravity and solar radiation parameters but decreases with augmenting the Prandtl number, magnetic field parameter, and porous medium parameter. It is deduced from the presented results that the temperature becomes lower by increasing the values of the reduced gravity parameter and the Prandtl number, but, on the other hand, it becomes higher by increasing the values of the magnetic field, the porous medium, and the radiation parameters at all the considered positions of the surface of the sphere. A comparison between the present and already published results is performed to check the validity of the proposed numerical model.

Keywords: reduced-gravity; porous-medium; magnetohydrodynamics; heat transfer; solar-radiation; finite difference method; sphere

Citation: Abbas, A.; Sarris, I.E.; Ashraf, M.; Ghachem, K.; Hnaien, N.; Alshammari, B.M. The Effects of Reduced Gravity and Radiative Heat Transfer on the Magnetohydrodynamic Flow Past a Non-Rotating Stationary Sphere Surrounded by a Porous Medium. *Symmetry* **2023**, *15*, 806. https://doi.org/10.3390/sym15040806

Academic Editors: Tomohiro Inagaki and Olga Kodolova

Received: 1 January 2023
Revised: 6 March 2023
Accepted: 22 March 2023
Published: 26 March 2023

1. Introduction

Researchers were interested in natural convection because of its importance in several natural phenomena and engineering applications. It occurs in the plume rising from fire air, as well as in ocean currents and other phenomena. Its primary use in the industrial sector is in free air cooling without the use of fans. Spherical-shaped components are important in both engineering and industrial applications. Kuiken and Merkin [1]

investigated the heat transfer process caused by heated bars while considering the influence of reduced gravity. Ostrach [2] studied the free convection along a vertical plate by focusing on the effect of the Grashof number on the temperature and velocity fields. Merkin [3] studied the free convection on a vertical flat plate at small Prandtl numbers. Lin [4] analyzed the natural convective heat transfer in a squared cavity filled with water at maximum density. Ivey and Hemblin [5] studied the free convection for large Rayleigh number values and small aspect ratios in 2D cavities. Potter and Riley [6] used a cloud-free model to study the natural convection across a stationary sphere at high Grashof numbers. Riley [7] investigated the free convection past a sphere under imposed conditions and parameters included in the model. Ashraf et al. [8] carried out a numerical study on the oscillatory heat transfer past a stationary sphere. By considering the fluid dissipation effects, Ashraf and Fatima [9] numerically solved the unsteady fluid flow and heat transfer along a sphere. A numerical investigation was presented by Ashraf et al. [10] to study the free convection of a nanofluid. Researchers in [11–16] explored the thermophoretic effects on convective heat transfer around a sphere by considering various fluid properties. Ahmad et al. [17] performed a computational study using the finite difference method to investigate the convective, chemically reacting heat transfer along a curved surface.

From a technological point of view, magnetohydrodynamic effects are crucial due to their diverse applications, including geophysics, electrical power generation, etc. The effect of an externally applied magnetic field on the boundary layer flow is getting a lot of attention from researchers. Several geometries with various boundary conditions have been considered to study MHD convective heat transfer. MHD Sakiadis flow on an inclined surface was quantitatively examined by Abbas et al. [18], with a focus on the influence of varying density. Tamoor et al. [19] examined the magnetohydrodynamic Casson fluid flow over a stretching cylinder. Pattnaik et al. [20] evaluated the effects of the magnetic field and chemical reaction on convective heat and mass transfers over an exponentially extending sheet. The Homotopy Analysis Method was used by Mabood et al. [21] to numerically solve the magnetohydrodynamic flow with thermal radiation effects over an exponentially stretched sheet. Khan et al. [22] presented a numerical study on the bioconvection flow along a paraboloid surface under MHD effects. Bulinda et al. [23] discussed the MHD free convective flow along a corrugated vibrating bottom surface with considering the effects of Hall currents. Alwawi et al. [24] performed a study on the MHD natural convection flow of a Casson nanofluid around a solid sphere. Chamkha et al. [25] studied the double diffusive magnetoconvection past a sphere.

Due to their significance in engineering and industrial applications, such as oil reservoirs, resin transfer models, porous insulation, packed beds, geothermal energy, fossil fuel beds, and nuclear waste disposal, the flows saturating porous space have drawn researchers' attention. Chitra and Kavitha [26] investigated the pulsatile flow in a circular pipe filled with a porous medium under the influence of a time-dependent pressure gradient. In [27–31], different processes of heat transfer and fluid flow on diverse geometries embedded in porous media have been carried out for various fluids. Hussain and Sheremet [32] carried out an analysis of the radiative nanofluid flow in porous media past a stretching surface under the influence of a magnetic field. Yan et al. [33] studied numerically a micro-combustor embedded in a porous medium. They concluded that the performance of such a device can be improved by increasing the thickness of the porous medium. In the presence of an anisotropic porous medium and stratified fluid, Jha et al. [34] presented semi-analytical results for transient natural convection fluid flow between two concentric vertical cylinders of infinite lengths. The laminar mixed convection in a porous channel with two distinct heat sources on the bottom wall was experimentally investigated by El-Kady [35]. The main goal was to demonstrate how the parameters of heat transfer are affected when a porous medium is used in the channel. For low values of the Prandtl number, Sparrow and Gregg [36] investigated free and forced convection flow across a flat plate.

Due to its diverse applications in industry, including boilers, rocket engines, nuclear reactor cooling, and thermal insulation, convective heat transfer, combined with thermal radiation effects, has attracted the attention of the research community. By taking into account radiation influence, Hossain and Thakkar [37] investigated the model of convective flow across an isothermal vertical plate. The MHD mixed convective flow on an isothermal surface submerged in a porous medium was the subject of a computational investigation performed by Damseh [38]. A study of the effects of thermal radiation on free convection through a permeable enclosure was considered by Zehamatkesh [39]. The radiative convective flow across a vertical plate submerged in a porous medium has been studied by Mondal et al. [40]. According to Muhammad et al. [41], micropolar fluid is impacted by heat generation, magnetic field, radiation, and chemical reaction as it flows through a porous moving surface. A study that focuses on the micropolar fluid flow with radiation action over a stretching sheet was considered by Bhattacharyya et al. [42]. The stagnation point flow of a micropolar fluid in the presence of radiation and a magnetic field was investigated by Pal et al. [43]. The MHD radiative mixed convection flow under an inclined surface was explored by Moradi et al. [44]. Sheikholeslami et al. [45] considered the effect of a magnetic field on the heat transfer and fluid flow in a nanofluid-filled semi-annulus. The effects of radiation and transpiration on the boundary layer flow of a micropolar fluid past a stretching sheet were discussed by Hussain et al. [46]. Mukhopadhyay et al. [47] investigated the boundary layer flow over an exponentially stretched sheet along with the effects of transpiration, radiation, and slip condition. Hayat et al. [48] investigated the thermally stratified radiative flow of third-grade fluid across a stretched surface. Parkesy et al. [49] studied the effect of radiation on transient magnetohydrodynamic flow between porous vertical channels of a micropolar fluid by applying a third-kind boundary condition. According to Uddin et al. [50], thermal radiation, heat generation, and absorption have an important impact on magnetohydrodynamic heat transfer in micropolar fluid past a wedge with Hall and ion-slip currents. Studies on the physics of thermal radiation on diverse fluid flow phenomena are discussed in [51–53].

Based on the above-described literature review, the combined effects of MHD, reduced gravity, and solar radiation on heat transfer and fluid flow along a stationary sphere embedded in a porous medium have not yet been considered. In the next sections, the mathematical formulation and solution process for this considered configuration are described. In addition, the results are presented in terms of temperature and velocity profiles.

2. Mathematical Formulation

Consider the viscous, steady, incompressible, two-dimensional, and natural convective flow past a non-rotating and stationary sphere. The reduced gravity, solar radiation, and applied magnetic field effects on optically dense thick fluid flow are considered in the current study. The magnetic field is normal to the flow direction. The coordinates along and normal to the flow are (x, y), and the corresponding velocity components are (u, v). The temperature at the surface is T_w, and away from the surface, the free-stream temperature is T_∞ with $T_w > T_\infty$. Following [1–3], the governing equations that are continuity, momentum, and energy equations are given as Figure 1:

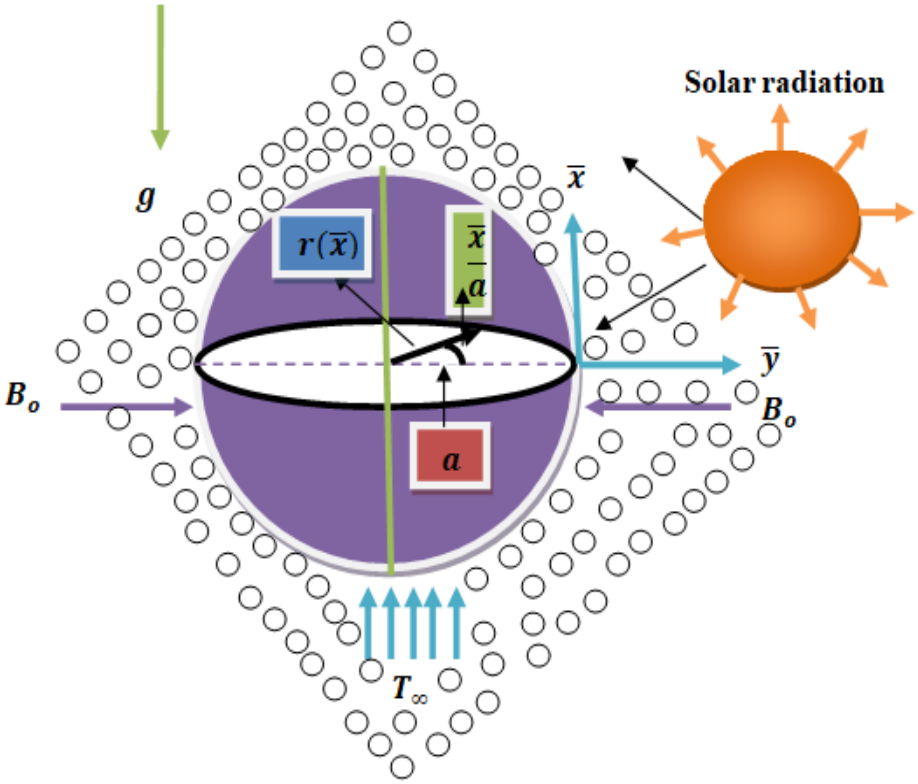

Figure 1. Considered configuration and Coordinate System.

$$\frac{\partial(\bar{r}\bar{u})}{\partial \bar{x}} + \frac{\partial(\bar{r}\bar{v})}{\partial \bar{y}} = 0, \tag{1}$$

$$\bar{u}\frac{\partial \bar{u}}{\partial \bar{x}} + \bar{v}\frac{\partial \bar{u}}{\partial \bar{y}} = \nu\frac{\partial^2 \bar{u}}{\partial \bar{y}^2} + g\frac{\rho-\rho_\infty}{\rho_\infty}sin\frac{\bar{x}}{a} - \frac{\sigma B_0^2}{\rho}u - \frac{\nu}{K_o}u, \tag{2}$$

$$\bar{u}\frac{\partial T}{\partial \bar{x}} + \bar{v}\frac{\partial T}{\partial \bar{y}} = \alpha_m\frac{\partial^2 T}{\partial \bar{y}^2} - \frac{1}{\rho C_p}\frac{\partial q_r}{\partial y}. \tag{3}$$

The distance from the symmetric axis to the sphere surface (radial distance) is $\bar{r} = a\,sin\frac{\bar{x}}{a}$. $(\bar{u}, \bar{v})$ are the velocity components toward and normal to the flow directions. The symbols $a, g, \rho, \nu, \sigma, B_0$, $\alpha_m = k/\rho C_P$, and K_0 designate the radius of the sphere, gravity acceleration, the density of the fluid, kinematic viscosity, thermal diffusivity, electrical conductivity, magnetic field, and permeability of the porous medium, respectively. In addition, k is the thermal conductivity of the fluid, and C_P is the specific heat at constant pressure.

Using the Rosseland approximation for radiation in an optically thick fluid, ref. [51–53], the radiative heat flux is simplified to:

$$q_r = -\frac{4\sigma}{3k^*}\frac{\partial T^4}{\partial y}. \tag{4}$$

k^* stands for average absorption coefficient, and σ is the Stefan-Boltzmann. The linearization of T^4 is given as follows:

$$T^4 \approx 4T_\infty^3 T - 3T_\infty^4.$$

Therefore, Equation (4) becomes:

$$q_r = -\frac{16T_\infty^3\sigma}{3K_R}\frac{\partial T}{\partial y}. \quad (5)$$

Thus, Equation (3) becomes:

$$u\frac{\partial T}{\partial x} + v\frac{\partial T}{\partial y} = \frac{k_\infty}{\rho C_p}\frac{\partial^2 T}{\partial y^2} + \frac{16T_\infty^3\sigma}{\rho C_P 3K_R}\frac{\partial^2 T}{\partial y^2}, \quad (6)$$

Further simplification of Equation (6) results in:

$$u\frac{\partial T}{\partial x} + v\frac{\partial T}{\partial y} = \frac{k}{\rho C_p}\frac{\partial}{\partial y}\left[\frac{\partial T}{\partial y} + \frac{4.4T_\infty^3\sigma}{\rho C_P 3kK_R}\frac{\partial T}{\partial y}\right], \quad (7)$$

The relationship between density and temperature, considering closeness of temperature to T_m, is as follows:

$$\frac{\rho-\rho_m}{\rho_m} = -\gamma(T - T_m)^2. \quad (8)$$

Furthermore, Equation (6) implies that for steady flow:

$$T \to T_m \pm \Delta T y \to \pm\infty \quad (9)$$

For fixed ΔT, consider the region $y \geq 0$ subject to the boundary conditions to obtain the symmetry conditions as:

$$\begin{gathered} \bar{u} = 0, \bar{v} = 0, T = T_m \text{ at } y = 0, \\ \bar{u} \to 0, T \to T_\infty \text{as } y \to \infty. \end{gathered} \quad (10)$$

where $T_\infty = T + \Delta T$ and is related to ρ_∞ by Equation (8). The reduced gravity is determined using the following expression:

$$g' = g\frac{(\rho_m - \rho_\infty)}{\rho_\infty} \quad (11)$$

From Equation (8), the fluid particles' acceleration having ρ_m as density becomes:

$$g' = g\gamma\frac{\rho_m}{\rho_\infty}(T_\infty - T_m)^2 \quad (12)$$

Moreover, the skin friction coefficient and the Nusselt number at the surface are expressed as follows:

$$C_f = \frac{\tau_w}{\rho U^2}, Nu = \frac{xq_w}{k(T_w - T_\infty)} \quad (13)$$

$$\text{Where } \tau_w = \mu\left(\frac{\partial \bar{u}}{\partial y}\right)_{y=0}, q_w = -k\left(\frac{\partial T}{\partial y}\right)_{y=0}, \quad (14)$$

3. Solution Methodology

In this section, the resolution of the above-presented governing equations with considered boundary conditions are described in detail.

3.1. Dimensionless Variables

The governing Equations (1)–(3) with boundary conditions (10) are put in their dimensionless forms using the following variables [13]:

$$x = \frac{\bar{x}}{a}, y = \frac{\bar{y}Gr^{\frac{1}{4}}}{a}, \theta = \frac{T - T_\infty}{T_m - T_\infty}, u = \frac{\bar{a}uGr^{\frac{1}{4}}}{\nu}, v = \frac{\bar{a}vGr^{\frac{1}{4}}}{\nu}, \quad (15)$$

When Equation (15) is used in Equations (1)–(3) with (10), they take the following form:

$$\frac{\partial(\sin x\, u)}{\partial x} + \frac{\partial(\sin x\, v)}{\partial y} = 0, \quad (16)$$

$$u\frac{\partial u}{\partial x} + v\frac{\partial u}{\partial y} = \frac{\partial^2 u}{\partial y^2} + R_g(2\theta - \theta^2)sinx - Mu - Ku \quad (17)$$

$$u\frac{\partial \theta}{\partial x} + v\frac{\partial \theta}{\partial y} = \frac{1}{Pr}\left(1 + \frac{4}{3}Rd\right)\frac{\partial^2 \theta}{\partial y^2}, \quad (18)$$

$$u = 0, v = 0, \theta = 1, \text{ at } y = 0, \quad u \to 0, \theta \to 0, \text{ as } y \to \infty. \quad (19)$$

Here, $R_g = \frac{g'}{g\beta\Delta T}, Rd = kk*/4\sigma^* T_\infty^3$, $\Pr = \frac{\nu}{\alpha}$, $K = \frac{a^2 Gr^{\frac{1}{4}}}{K_o} M = \frac{\sigma B_0^2 a^2 Gr^{\frac{1}{4}}}{\rho\nu}$ are reduced gravity, the radiation parameter, the Prandtl number, the porosity parameter, and the magnetic field parameter, respectively. Here, g' is reduced gravity acceleration defined in Equation (12).

3.2. Primitive Variable Formulation

Before using the finite difference method (FDM), Equations (16)–(19) are transformed into a smooth form, and a numerical algorithm is written using FORTRAN programming language. The following variables are defined as [13]:

$$u(x,y) = x^{1/2}U(X,Y), v(x,y) = x^{-\frac{1}{4}}V(X,Y), Y = x^{-\frac{1}{4}}y, X = x,, \theta(x,y) = \theta(X,Y). \quad (20)$$

By putting Equation (20) in Equations (16)–(19), the governing equations are expressed as:

$$XUcosX + (X\frac{\partial U}{\partial X} - \frac{Y}{2}\frac{\partial U}{\partial Y} + \frac{\partial V}{\partial Y})sinX = 0, \quad (21)$$

$$XU\frac{\partial U}{\partial X} + \frac{1}{2}U^2 + \left(V - \frac{YU}{2}\right)\frac{\partial U}{\partial Y} = \frac{\partial^2 U}{\partial Y^2} + R_g(2\theta - \theta^2)sinX - MU - KU \quad (22)$$

$$XU\frac{\partial \theta}{\partial X} + \left(V - \frac{YU}{2}\right)\frac{\partial \theta}{\partial Y} = \frac{1}{Pr}\left(1 + \frac{4}{3}Rd\right)\frac{\partial^2 \theta}{\partial Y^2} \quad (23)$$

The corresponding boundary conditions are:

$$U = 0, V = 0, \theta = 1, \text{at } Y = 0, \quad U \to 0, \theta \to 0, asY \to \infty. \quad (24)$$

3.3. Solution Scheme

The governing Equations (21)–(23) are discretized using the finite difference method. The X-axis is used to apply the backward difference, while the Y-axis is used to apply the central difference. After the flow equations are discretized, the unknown variables $(U_{i,j}, V_{i,j}, \theta_{i,j})$ are evaluated based on the boundary conditions specified in (24). The discretization is performed as follows:

$$\frac{\partial U}{\partial X} = \frac{U_{(i,j)} - U_{(i,j-1)}}{\Delta X}, \tag{25}$$

$$\frac{\partial U}{\partial Y} = \frac{U_{(i+1,j)} - U_{(i,-1,j)}}{2\Delta Y}, \tag{26}$$

$$\frac{\partial^2 U}{\partial Y^2} = \frac{U_{(i+1,j)} - 2U_{(i,j)} + U_{(i,-1,j)}}{\Delta Y^2}. \tag{27}$$

Discretized Continuity equation:

$$V_{(i+1,j)} = V_{(i-1,j)} - 2\frac{\Delta Y}{\Delta X} X_i \left(U_{(i,j)} - U_{(i,j-1)}\right) + \frac{Y_j}{2}\left(U_{(i+1,j)} - U_{(i-1,j)}\right) - 2\Delta Y X_i \frac{cosX_i}{sin\, X_i} U_{(i,j)}, \tag{28}$$

Discretized Momentum equation:

$$\left(1 + \tfrac{\Delta Y}{2}\left(V_{(i,j)} - \tfrac{Y_j}{2}U_{(i,j)}\right)\right)U_{(i-1,j)} + \left(-2 - \tfrac{\Delta Y^2}{\Delta X}X_i U_{(i,j)} - M - K\right)U_{(i,j)} + \left(1 - \tfrac{\Delta Y}{2}\left(V_{(i,j)} - \tfrac{Y_j}{2}U_{(i,j)}\right)\right)U_{(i+1,j)} = -\Delta Y^2 sinX_i R_g(2\theta_{(i,j)} - \theta^2{}_{(i,j)}), \tag{29}$$

Discretized Energy equation:

$$\left(\tfrac{1}{Pr}(1 + \tfrac{4}{3}Rd) + \tfrac{\Delta Y}{2}\left(V_{(i,j)} - \tfrac{Y_j}{2}U_{(i,j)}\right)\right)\theta_{(i-1,j)} + \left(-\tfrac{2}{Pr}(1 + \tfrac{4}{3}Rd) + \Delta Y^2 U_{(i,j)}\left(1 - \tfrac{X_i}{\Delta X}\right)\right)\theta_{(i,j)} + \left(\tfrac{1}{Pr}(1 + \tfrac{4}{3}Rd) - \tfrac{\Delta Y}{2}\left(V_{(i,j)} - \tfrac{Y_j}{2}U_{(i,j)}\right)\right)\theta_{(i+1,j)} = -\tfrac{\Delta Y^2}{\Delta X}X_i U_{(i,j)}\theta_{(i,j-1)}, \tag{30}$$

Discretized Boundary Conditon:

$$U_{i,j} = 0, V_{i,j} = 0, \theta_{i,j} = 1, \text{at} Y_j = 0, \quad U_{i,j} \to 0, \theta_{i,j} \to 0, as Y_j \to \infty. \tag{31}$$

The approximate solutions determined with the finite difference method are discussed in detail in the forthcoming section. The convergence criterion used to achieve accurate numerical solutions for the variables U, V, θ, and ϕ, respectively, is presented as follows:

$$max|U_{ij}| + max|V_{ij}| + max|\theta_{ij}| \leq \epsilon,$$

where $\epsilon = 10^{-5}$. The computation is started at $X = 0$ and then goes downstream implicitly. The step sizes are taken as: $\Delta X = 0.05$ and $\Delta Y = 0.02$.

4. Results and Discussion

The numerical results of the studied configuration are presented and discussed in detail in the current section. Results are presented in term of the profiles of velocity U and temperature θ; skin friction $\partial U/\partial Y$ and heat transfer rate $\partial\theta/\partial Y$ for different values of reduced gravity number R_g, Prandtl number Pr, thermal radiation parameter Rd, magnetic field parameter M, and porous medium parameter K are computed and presented in the form of graphs and tables.

The effects of the reduced gravity parameter R_g on the velocity profile U for Prandtl number Pr = 7.0 at various points on the sphere are shown in Figure 2. The graph shows that when R_g is improved, the velocity profile U increases. The numerical results of fluid temperature for various values of R_g are shown in Figure 3. The temperature curves show that the fluid temperature rapidly decreases as R_g is strengthened, at all the considered points. The maximum temperature magnitude occurs at $X = \pi$. From a physical point of view, the increase of the reduced gravity parameter leads to a decrease in thermal expansion and thus a smaller temperature difference between the surface and the surrounding fluid, which results in a decrease in the fluid flow domain's overall temperature. Figures 4 and 5 present the effect of the porous medium parameter on the velocity and temperature profiles, respectively. Figure 4 highlights the influence of the porous medium parameter K on the velocity field. It shows that as K is increased, U decreases at all the considered positions. Figure 5 depicts the behavior of θ for various values of K. It is noticed that as K is raised, θ increases. The velocity and temperature profiles for various values of the solar radiation parameter Rd are shown in Figures 6 and 7 at various locations around the sphere. It should be mentioned that velocity and temperature increase when Rd is increased**.** Physically, these results are due to the enhancement of the overall heat transfer coefficient and absorption efficiency, which contribute to raising the temperature of the fluid flow domain. The effects of the magnetic field parameter M on the temperature and velocity fields are shown in Figures 8 and 9. With the intensification of M, it can be observed that the velocity is reduced, and the temperature is increasing. This fact is physically due to the generated Lorentz force caused by the interaction between the magnetic field and the flow motion. This force reduces the flow intensity, and because of the produced viscous resistance, the fluid's temperature rises.

The velocity profiles for various values of Pr are sketched in Figure 10. The increase of Pr leads to the decrease of velocity, due to the enhancement of the viscous dissipations. The highest value for U is achieved at $X = \frac{\pi}{2}$. Figure 11 shows the effects of Pr on θ. The results indicate that the temperature of the fluid reduces as Pr is increased. From a physical point of view, this is due to the reduction of the thermal conductivity of the fluid that causes the reduction of temperature. The kinematic viscosity is increased by increasing Pr, and, as a result, the viscous effects become stronger, and the velocity of the fluid decreases. Table 1 is showing the numerical results of skin friction $\partial U/\partial Y$ and the rate of heat transfer $\partial\theta/\partial Y$ for different values of reduced gravity parameter R_g when the remaining parameters are kept constant. It is deduced that as R_g is increased, both skin friction and the rate of heat transfer become stronger at the leading edge $Y = 0$. It is noted that all the results satisfy the given boundary conditions. Table 2 presents the comparison of the present results concerning skin friction with already published results for special cases, and it is observed that there is excellent agreement. This confirms the validity of the current numerical model.

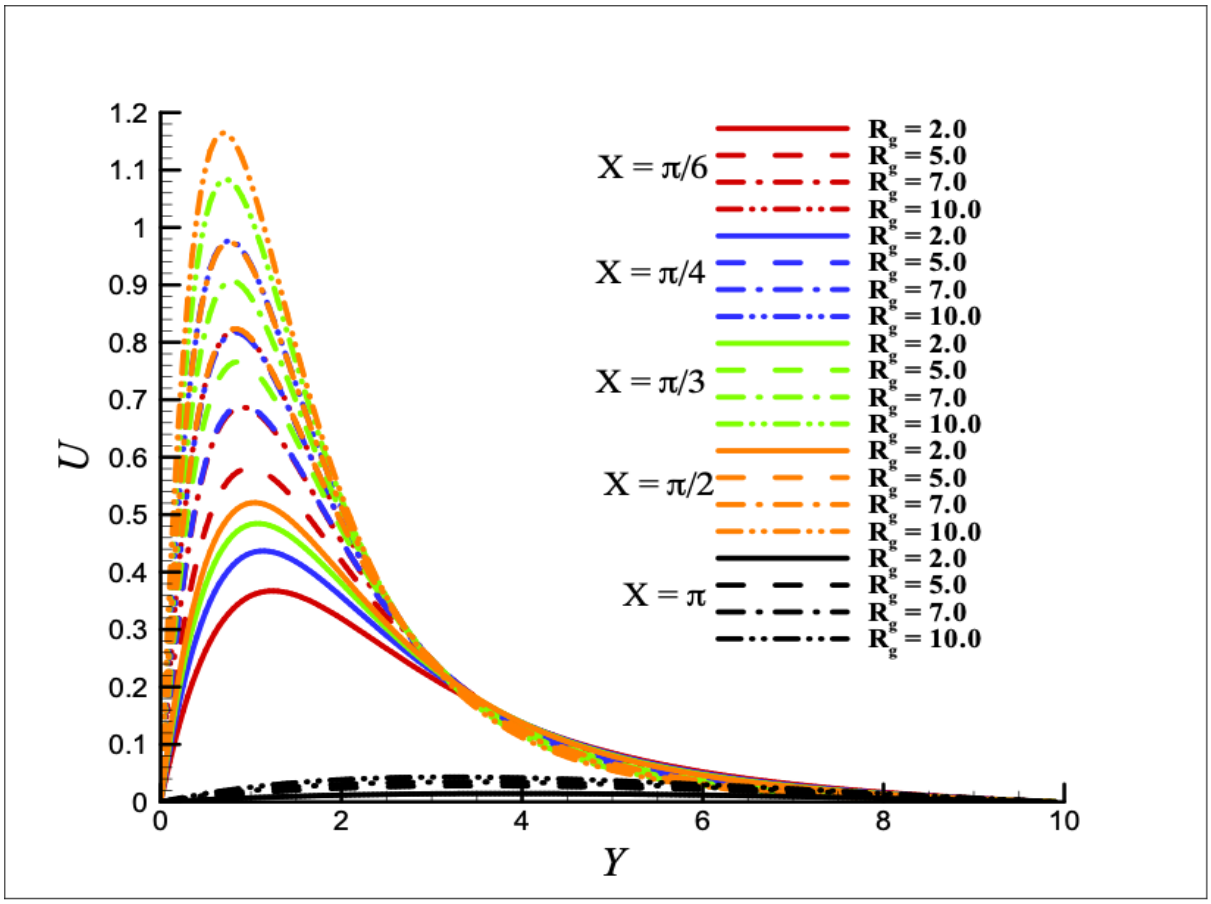

Figure 2. Effect of R_g on U when Pr = 7.0, $Rd = 1.0$, $K = 0.1$, and $M = 1.0$.

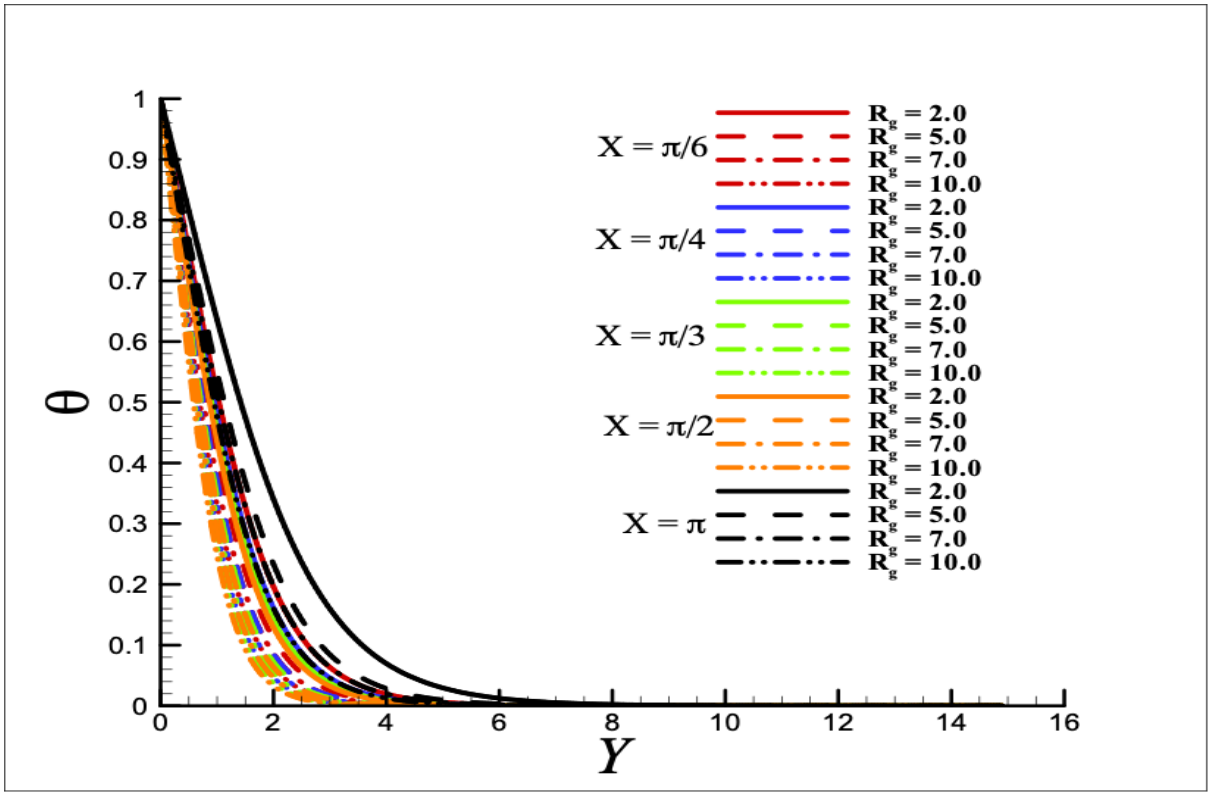

Figure 3. Effect of R_g on θ when Pr = 7.0, $Rd = 1.0$, $K = 0.1$, and $M = 1.0$.

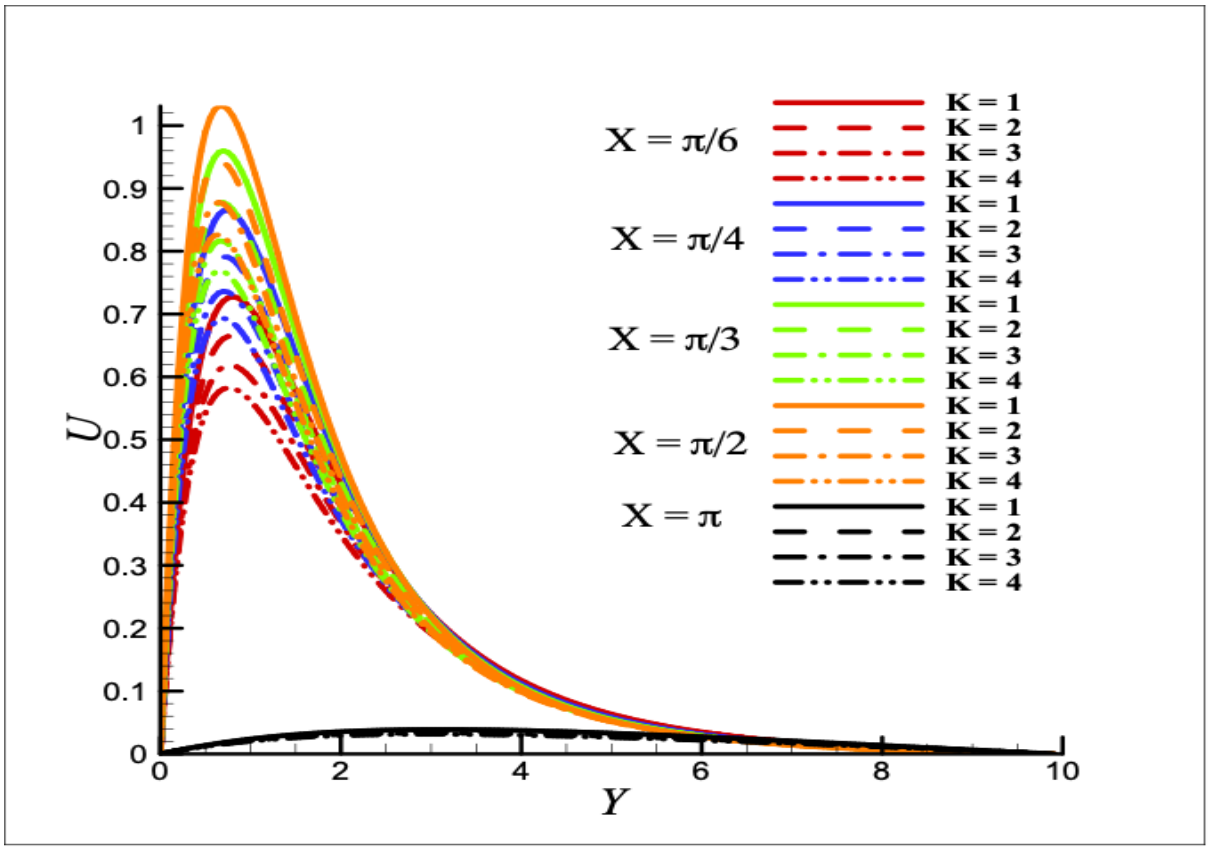

Figure 4. Effect of K on U when R_g =10.0, Rd = 1.0, Pr = 7.0, and M = 1.0.

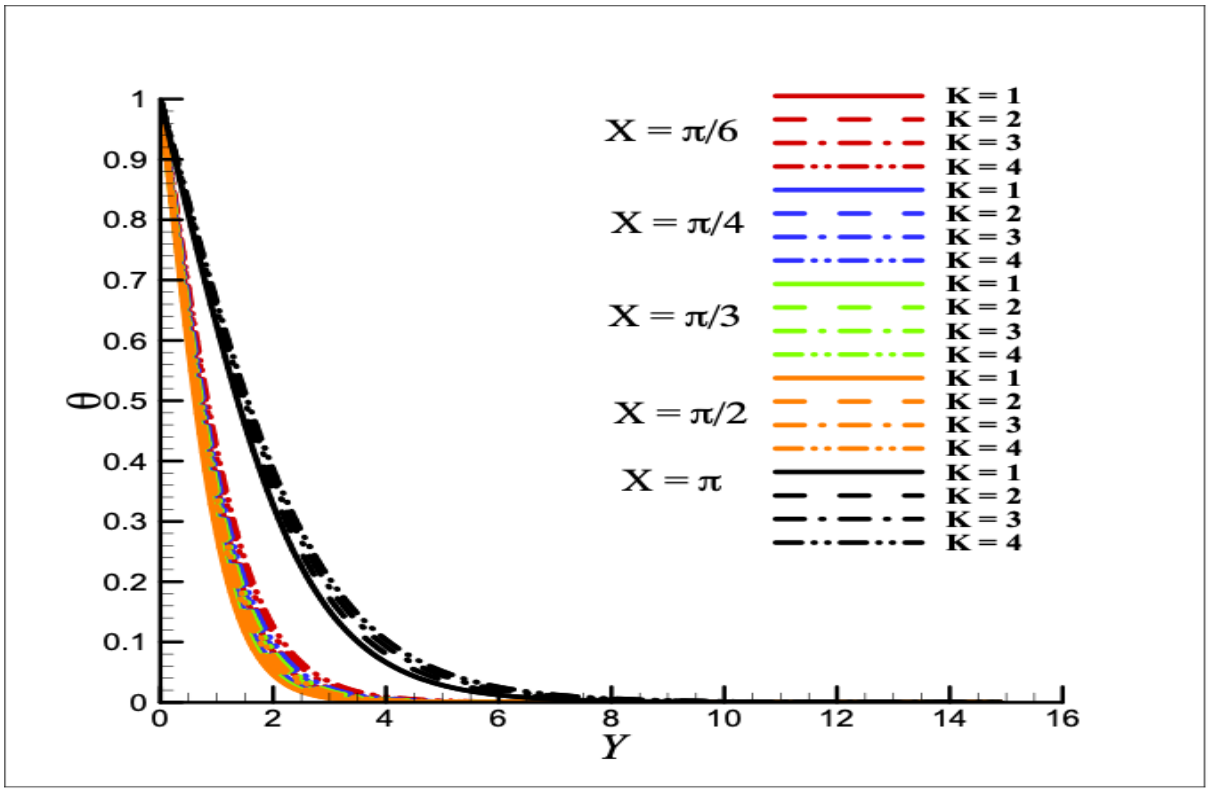

Figure 5. Effect of K on θ when R_g =10.0, Rd = 1.0, Pr = 7.0, and M = 1.0.

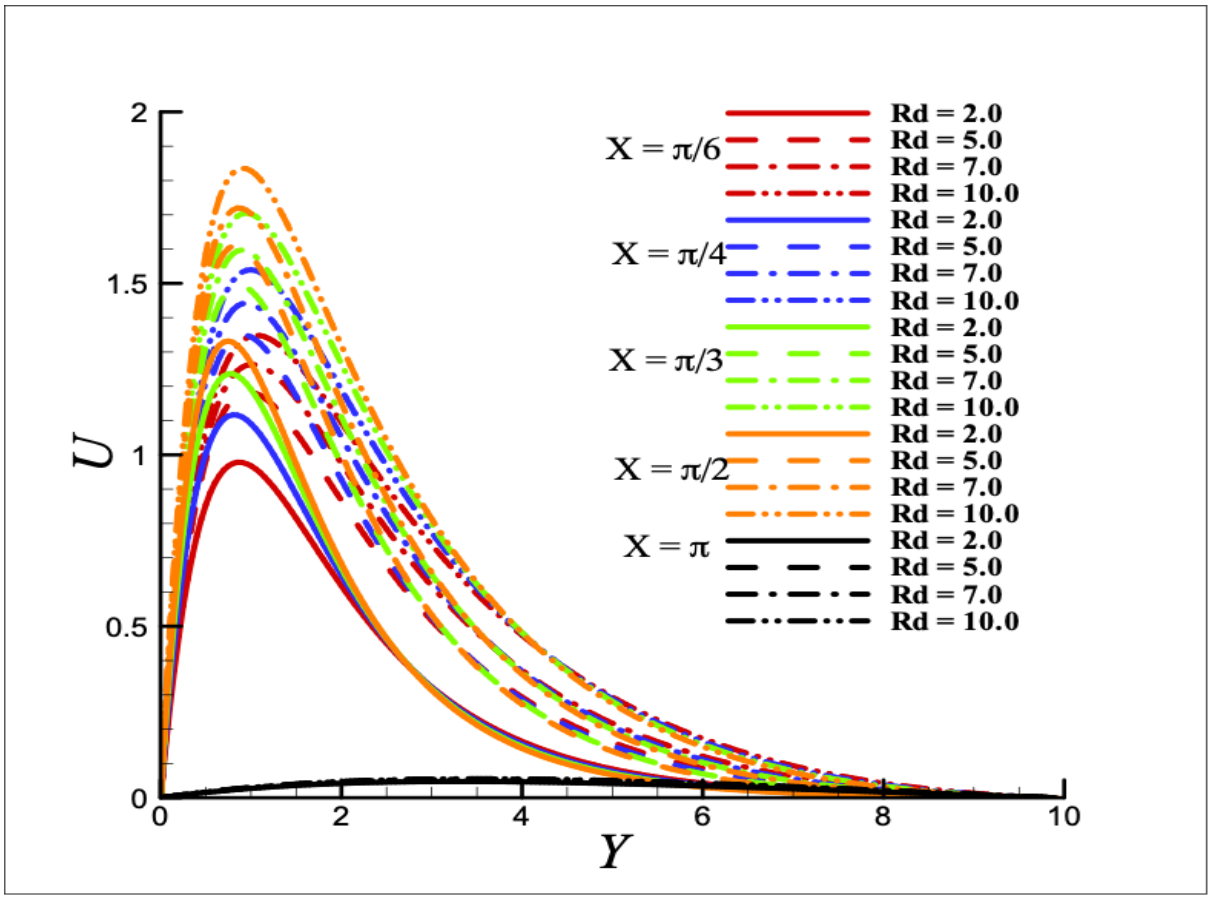

Figure 6. Effect of Rd on U when R_g =10.0, Pr = 7.0, K = 0.1, and M = 1.0.

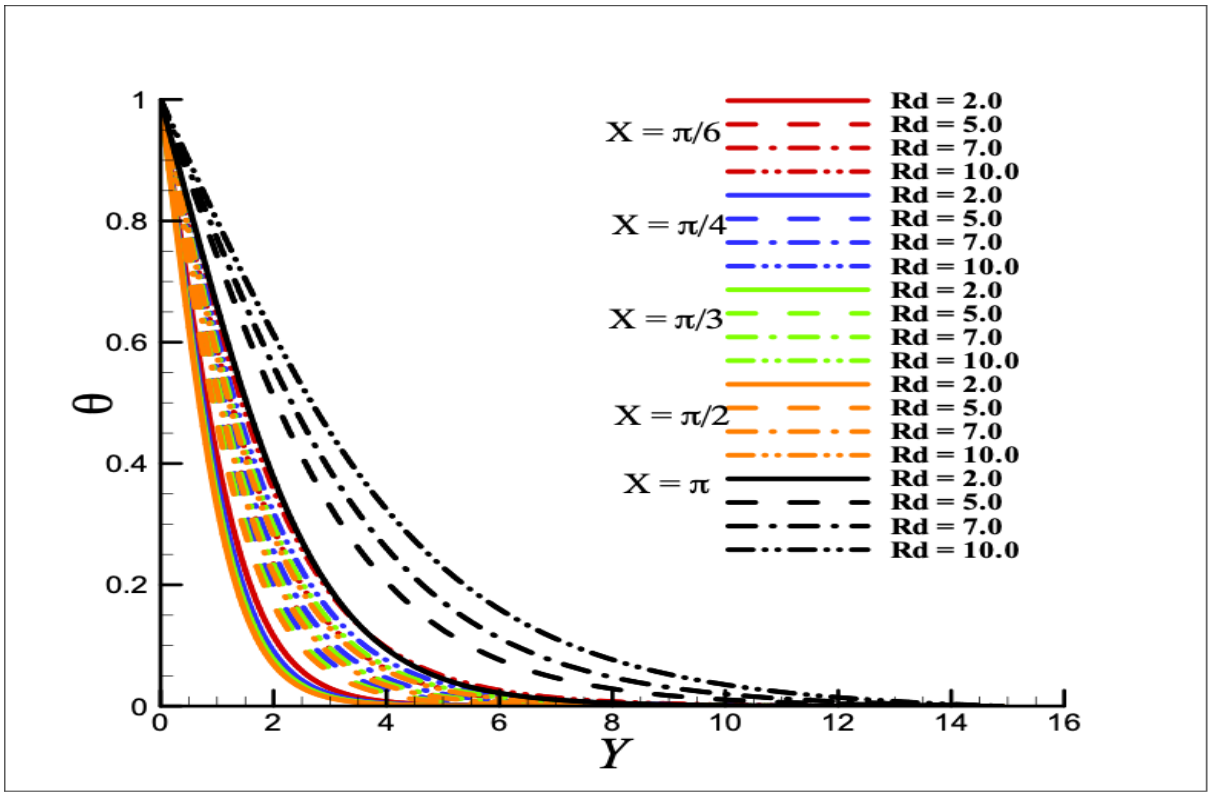

Figure 7. Effect of Rd on θ when R_g =10.0, Pr = 7.0, K = 0.1, and M = 1.0.

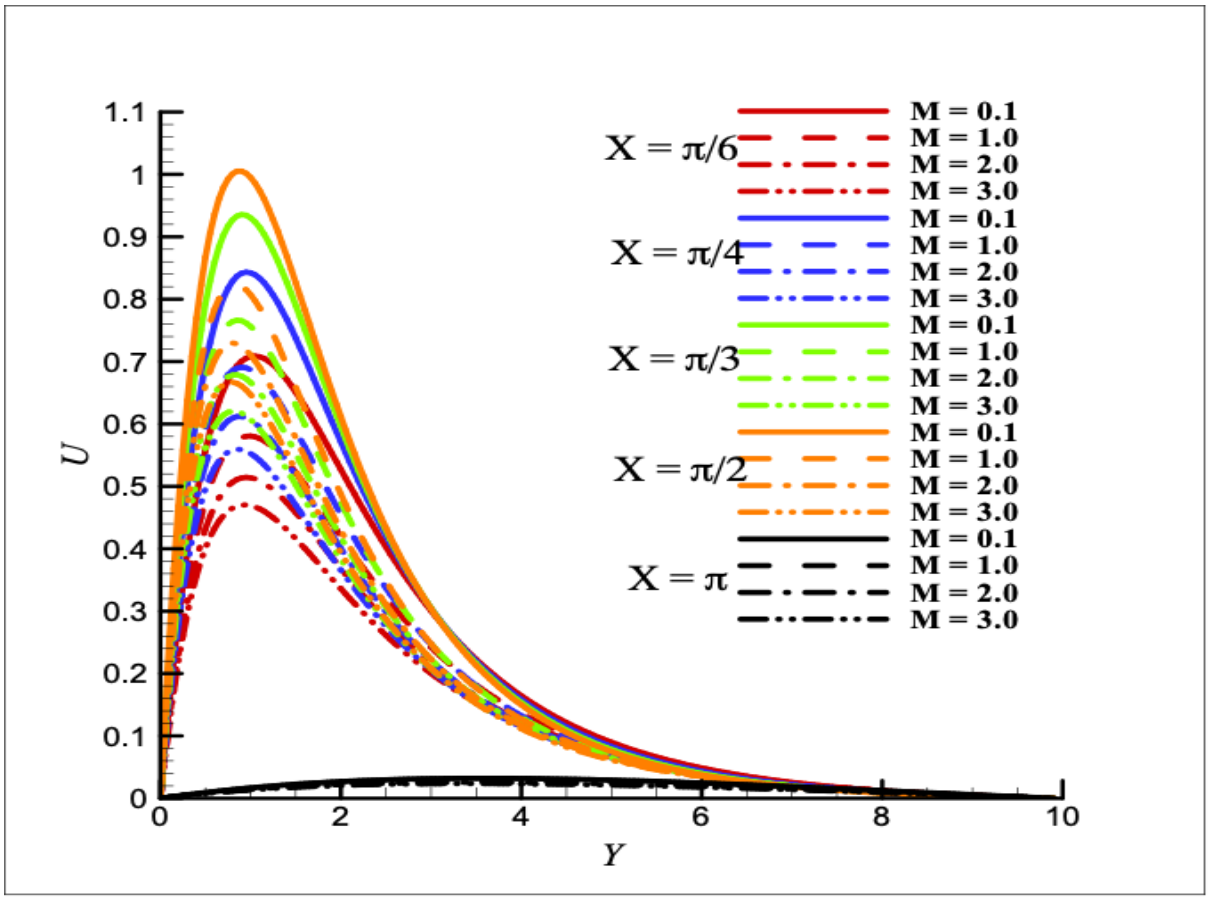

Figure 8. Effect of M on U when R_g =10.0, Pr = 7.0, K = 0.1, and Rd = 1.0.

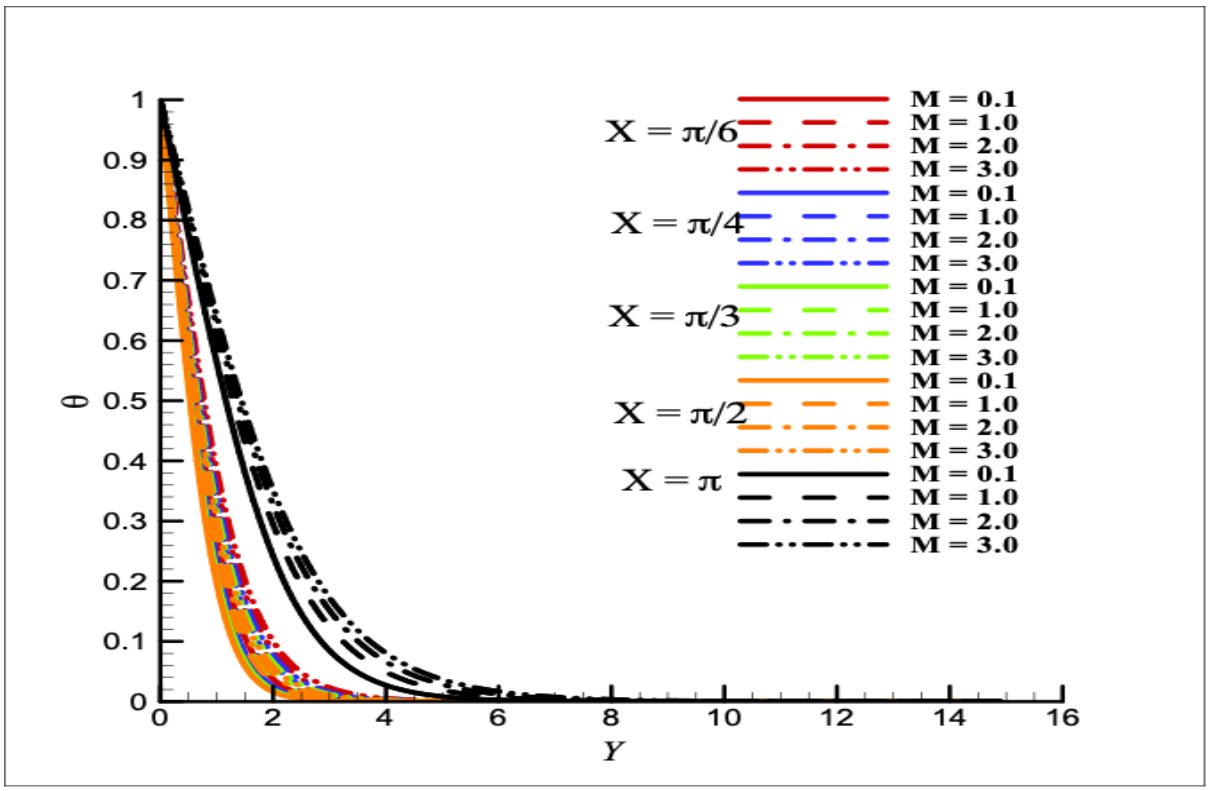

Figure 9. Effect of M on θ when R_g =10.0, Pr = 7.0, K = 0.1, and Rd = 1.0.

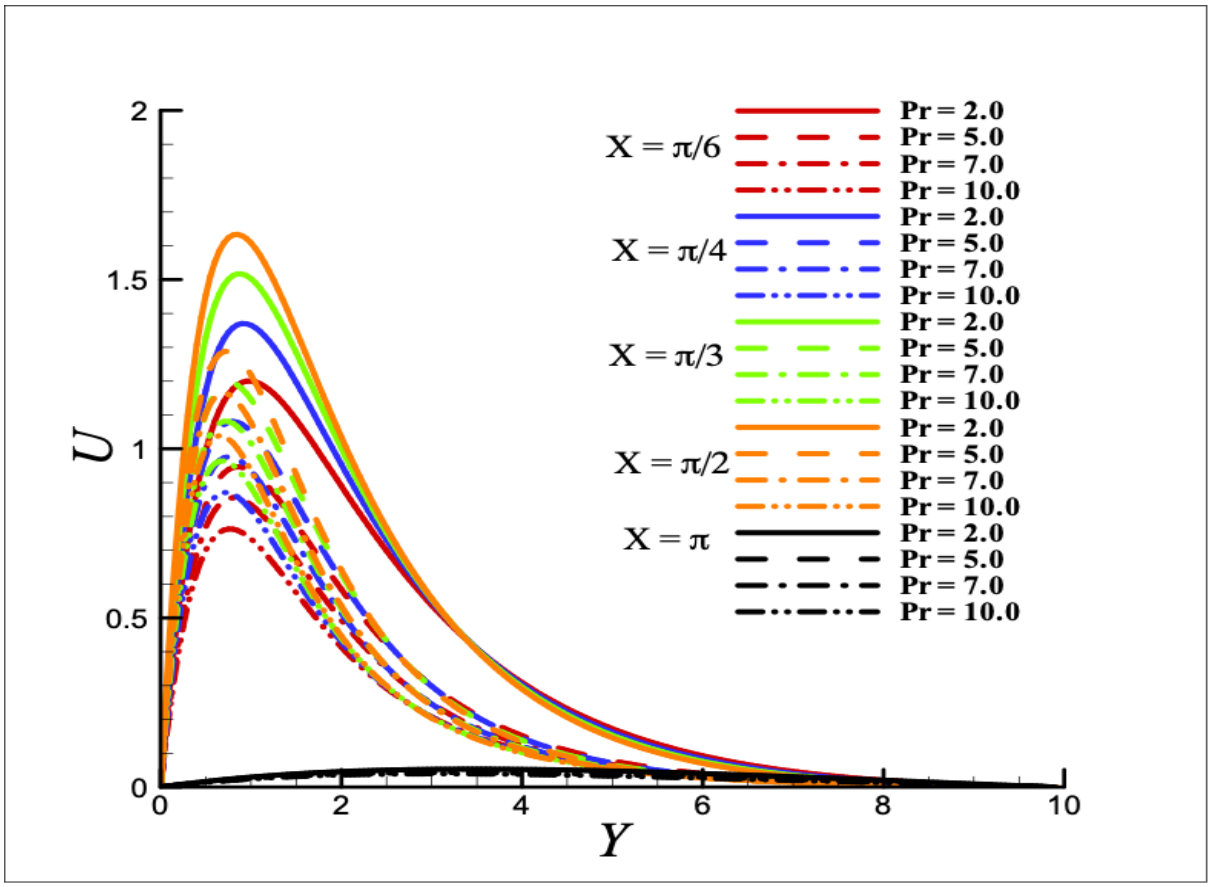

Figure 10. Effect of Pr on U when $R_g = 10.0$, $M = 1.0$, K = 0.1, and $Rd = 1.0$.

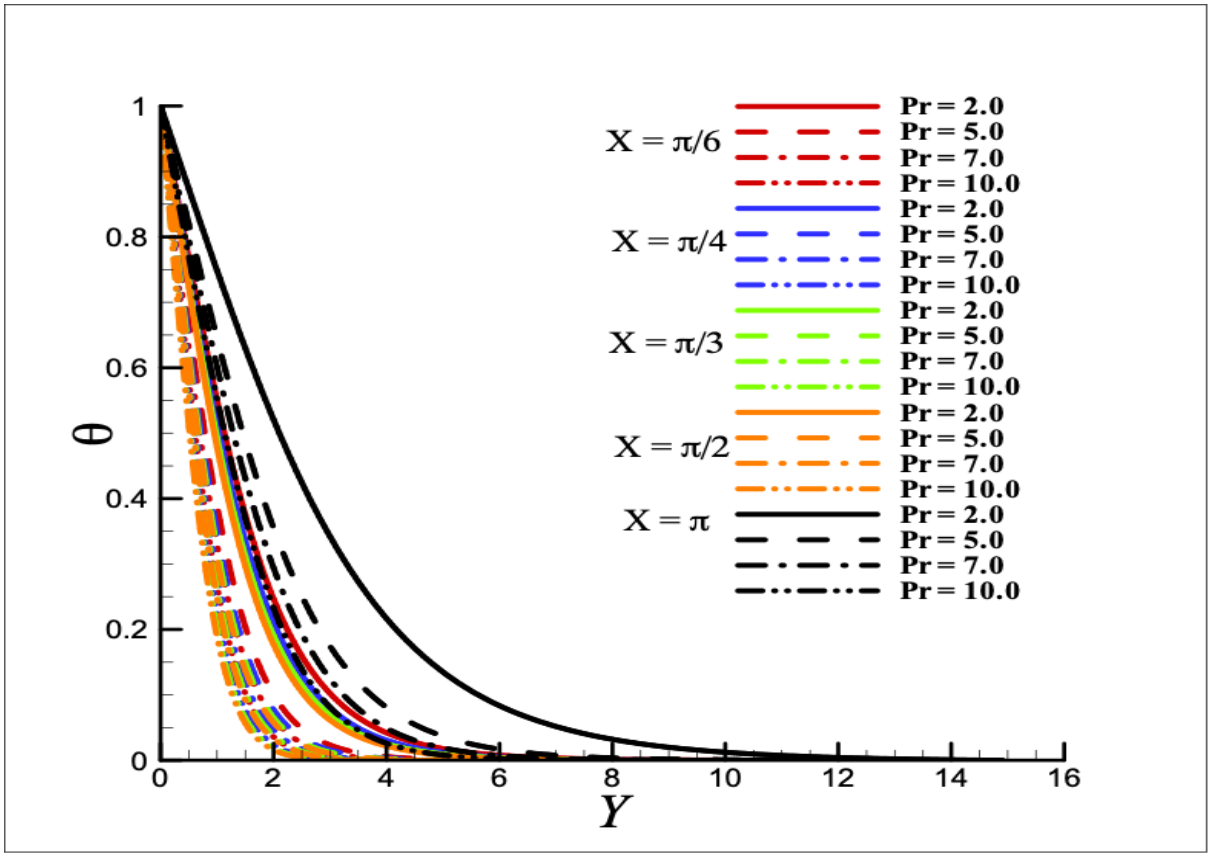

Figure 11. Effect of Pr on θ when $R_g = 10.0$, $M = 1.0$, K = 0.1, and $Rd = 1.0$.

Table 1. Effect of Pr on $(a)\left(\frac{\partial U}{\partial Y}\right)_{Y=0}$ $(b)-\left(\frac{\partial \theta}{\partial Y}\right)_{Y=0}$ for different values of R_g, $M = 0.1$, K = 0.1, and $Rd = 0.1, Pr = 7.0$.

R_g	$\left(\frac{\partial U}{\partial Y}\right)_{Y=0}$	$-\left(\frac{\partial \theta}{\partial Y}\right)_{Y=0}$
0.1	0.07511	0.32437
0.5	0.25270	0.49175
0.7	0.32540	0.53556
0.9	0.39301	0.57069
1.0	0.42536	0.58607
2.0	0.71561	0.69778
5.0	1.42254	0.87804
10.0	2.39128	1.04443

Table 2. Comparison of the results of $\left(\frac{\partial U}{\partial Y}\right)_{Y=0}$ with those of Sparrow & Gregg [36] when reduced gravity term is absent for $M = 0, Rd = 0, K = 0at\ \pi/2$.

Pr	Sparrow & Gregg [36]	Present
0.03	0.93841	0.93740
0.02	0.95896	0.95870
0.008	0.99550	0.99400

5. Conclusions

The effects of reduced gravity, solar radiation, and an external magnetic field on the heat transfer and fluid flow past a stationary and non-rotating sphere submerged in a fluid and embedded in a porous medium is discussed in the current work. The main findings are summarized as follows:

- When $R_g$is increased, U increases at all the points on the sphere, and the maximum value occurs at $X = \frac{\pi}{2}$. As R_g is increased, the buoyancy force increases and accelerates the fluid motion. Also, the velocity increases with increasing the values of porous medium parameter K.
- The increase in R_g results in the reduction of θ, and the maximum value is obtained at $X = \pi$.
- The increase of Pr leads to a decrease of velocity and temperature, due to the enhancement of viscous effects and the reduction of thermal conductivity.
- The augmentation of Rd, K, and M cause the raising of temperature and the reduction of velocity.
- Skin friction and heat transfer rate increase with increasing the values of R_g.
- The verification of the used numerical model is performed by comparing it to previously published results on skin friction, and good agreement is encountered.

Author Contributions: Conceptualization, A.A. and M.A.; methodology, A.A.; software, A.A.; validation, I.E.S., K.G. and N.H.; formal analysis, B.M.A.; investigation, M.A.; resources, K.G.; data curation, I.E.S.; writing—original draft preparation, A.A.; writing—review and editing, N.H.; visualization, B.M.A.; supervision, M.A.; project administration, K.G.; funding acquisition, B.M.A. All authors have read and agreed to the published version of the manuscript.

Funding: Princess Nourah bint Abdulrahman University Researchers Supporting Project number (PNURSP2023R41), Princess Nourah bint Abdulrahman University, Riyadh, Saudi Arabia.

Institutional Review Board Statement: Not applicable.

Informed Consent Statement: Not applicable.

Data Availability Statement: Not applicable.

Conflicts of Interest: Authors declare no conflict of interest.

References

1. Kay, A.; Kuiken, H.K.; Merkin, J.H. Boundary-layer analysis of the thermal bar. *J. Fluid Mech.* **1995**, *303*, 253–278.
2. Ostrach, S. *An Analysis of Laminar Free-Convection Flow and Heat Transfer about a Flat Plate Parallel to the Direction of the Generating Body Force*; National Aeronautics and Space Administration Cleveland Oh Lewis Research Center: Cleveland, OH, USA, 1952.
3. Merkin, J.H. Free convection on a heated vertical plate: The solution for small Prandtl number. *J. Eng. Math.* **1989**, *23*, 273–282.
4. Lin, D.S.; Nansteel, M.W. Natural convection heat transfer in a square enclosure containing water near its density maximum. *Int. J. Heat Mass Transf.* **1987**, *30*, 2319–2329.
5. Ivey, G.N.; Hamblin, P.F. Convection near the temperature of maximum density for high Rayleigh number, low aspect ratio, rectangular cavities. *ASME J. Heat Transfer.* **1989**, *111*, 100–105
6. Potter, J.M.; Riley, N. Free convection from a heated sphere at large Grashof number. *J. Fluid Mech.* **1980**, *100*, 769–783.
7. Riley, N. The heat transfer from a sphere in free convective flow. *Comput. Fluids* **1986**, *14*, 225–237.
8. Ashraf, M.; Fatima, A.; Gorla, R.S.R. Periodic momentum and thermal boundary layer mixed convection flow around the surface of a sphere in the presence of viscous dissipation. *Can. J. Phys.* **2017**, *95*, 976–986.
9. Ashraf Mand Fatima, A. Numerical simulation of the effect of transient shear stress and the rate of heat transfer around different positions of sphere in the presence of viscous dissipation. *J. Heat Transf.* **2018**, *140*, 701–7012.
10. Ashraf, M.; Khan, A.; Gorla, R.S.R. Natural convection boundary layer flow of nanofluids around different stations of the sphere and into the plume above the sphere. *Heat Transf.—Asian Res.* **2019**, *48*, 1127–1148.
11. Abbas, A.; Ashraf, M.; Chu, Y.; Zia, S.; Khan, I.; Nisar, K.S. Computational Study of the Coupled Mechanism of Thermophoretic Transportation and Mixed Convection Flow around the Surface of a Sphere. *Molecules* **2020**, *25*, 2694.
12. Abbas, A.; Muhammad, A. Combined effects of variable viscosity and thermophoretic transportation on mixed convection flow around the surface of a sphere. *Therm. Sci.* **2020**, *24*, 4089–4101.
13. Ashraf, M.; Abbas, A.; Ali, A.; Shah, Z.; Alrabaiah, H.; Bonyah, E. Numerical simulation of the combined effects of thermophoretic motion and variable thermal conductivity on free convection heat transfer. *AIP Adv.* **2020**, *10*, 085005.
14. Abbas, A.; Ashraf, M.; Chamkha, A.J. Combined effects of thermal radiation and thermophoretic motion on mixed convection boundary layer flow. *Alex. Eng. J.* **2021**, *60*, 3243–3252.
15. Ashraf, M.; Abbas, A.; Zia, S.; Chu, Y.M.; Khan, I.; Nisar, K.S. Computational analysis of the effect of nano particle material motion on mixed convection flow in the presence of heat generation and absorption. *Comput. Mater. Contin.* **2020**, *65*, 1809–1823.
16. Ashraf, M.; Abbas, A.; Oztop, H.F.; Nisar, K.S.; Khan, I. Computations of mixed convection slip flow around the surface of a sphere: Effects of thermophoretic transportation and viscous dissipation. *Heat Transf.* **2021**, *50*, 7349–7362.
17. Ahmad, U.; Ashraf, M.; Abbas, A.; Rashad, A.M.; Nabwey, H.A. Mixed convection flow along a curved surface in the presence of exothermic catalytic chemical reaction. *Sci. Rep.* **2021**, *11*, 12907.
18. Abbas, A.; Ijaz, I.; Ashraf, M.; Ahmad, H. Combined effects of variable density and thermal radiation on MHD Sakiadis flow. *Case Stud. Therm. Eng.* **2021**, *28*, 101640.
19. Tamoor, M.; Waqas, M.; Khan, M.I.; Alsaedi, A.; Hayat, T. Magnetohydrodynamic flow of Casson fluid over a stretching cylinder. *Results Phys.* **2017**, *7*, 498–502.
20. Pattnaik, P.K.; Mishra, S.R.; Barik, A.K.; Mishra, A.K. Influence of chemical reaction on magnetohydrodynamic flow over an exponential stretching sheet: A numerical study. *Int. J. Fluid Mech. Res.* **2020**, *47*, 217–228.
21. Mabood, F.; Khan, W.A.; Ismail, A.M. MHD flow over exponential radiating stretching sheet using homotopy analysis method. *J. King Saud Univ.-Eng. Sci.* **2017**, *29*, 68–74.
22. Khan, M.; Salahuddin, T.; Malik, M.Y.; Alqarni, M.S.; Alqahtani, A.M. Numerical modeling and analysis of bioconvection on MHD flow due to an upper paraboloid surface of revolution. *Phys. A Stat. Mech. Its Appl.* **2020**, *553*, 124231.
23. Bulinda, V.M.; Kang'ethe, G.P.; Kiogora, P.R. Magnetohydrodynamics Free Convection Flow of Incompressible Fluids over Corrugated Vibrating Bottom Surface with Hall Currents and Heat and Mass Transfers. *J. Appl. Math.* **2020**, *2020*, 2589760.
24. Alwawi, F.A.; Alkasasbeh, H.T.; Rashad, A.M.; Idris, R. MHD natural convection of Sodium Alginate Cassonnanofluid over a solid sphere. *Results Phys.* **2020**, *16*, 102818.

25. Chamkha, A. Double-Diffusion MHD free convective flow along a sphere in the presence of a homogeneous chemical reaction and Soret and Dufour effects. *Appl. Comput. Math.* **2017**, *6*, 34–44. https://doi.org/10.11648/j.acm.20170601.12.
26. Chitra, M.; Kavitha, V. Pulsatile flow through a circular pipe with porous medium under the influence of time varying pressure gradient: Effects of with and without visco-elastic fluid. *Malaya J. Mat.* **2020**, *S*, 126–132.
27. Abbas, A.; Jeelani, M.B.; Alharthi, N.H. Magnetohydrodynamic Effects on Third-Grade Fluid Flow and Heat Transfer with Darcy–Forchheimer Law over an Inclined Exponentially Stretching Sheet Embedded in a Porous Medium. *Magnetochemistry* **2022**, *8*, 61.
28. Abbas, A.; Jeelani, M.B.; Alharthi, N.H. Darcy–Forchheimer Relation Influence on MHD Dissipative Third-Grade Fluid Flow and Heat Transfer in Porous Medium with Joule Heating Effects: A Numerical Approach. *Processes* **2022**, *10*, 906.
29. Abbas, A.; Shafqat, R.; Jeelani, M.B.; Alharthi, N.H. Convective Heat and Mass Transfer in Third-Grade Fluid with Darcy–Forchheimer Relation in the Presence of Thermal-Diffusion and Diffusion-Thermo Effects over an Exponentially Inclined Stretching Sheet Surrounded by a Porous Medium: A CFD Study. *Processes* **2022**, *10*, 776.
30. Abbas, A.; Shafqat, R.; Jeelani, M.B.; Alharthi, N.H. Significance of Chemical Reaction and Lorentz Force on Third-Grade Fluid Flow and Heat Transfer with Darcy–Forchheimer Law over an Inclined Exponentially Stretching Sheet Embedded in a Porous Medium. *Symmetry* **2022**, *14*, 779.
31. Abbas, A.; Jeelani, M.B.; Alnahdi, A.S.; Ilyas, A. MHD Williamson Nanofluid Fluid Flow and Heat Transfer Past a Non-Linear Stretching Sheet Implanted in a Porous Medium: Effects of Heat Generation and Viscous Dissipation. *Processes* **2022**, *10*, 1221.
32. Hussain, M.; Sheremet, M. Convection analysis of the radiative nanofluid flow through porous media over a stretching surface with inclined magnetic field. *Int. Commun. Heat Mass Transf.* **2023**, *140*, 106559.
33. Yan, Y.; Zhang, C.; Wu, G.; Feng, S.; Yang, Z. Numerical study on methane/air combustion characteristics in a heat-recirculating micro combustor embedded with porous media. *Int. J. Hydrog. Energy* **2022**, *47*, 20999–21012
34. Jha, B.K.; Musa, M.K. The combined effects of anisotropic porous medium and stably stratified fluid on free convective flow through an annulus. *J. Taibah Univ. Sci.* **2018**, *12*, 678–686.
35. El-Kady, M.S. Enhancement of Mixed Convection in a Channel with Discrete Heat Sources by Using a Highly Conducting Porous Medium.(Dept. M). *MEJ. Mansoura Eng. J.* **2021**, *25*, 1–6.
36. Sparrow, E.M.; Gregg, J.L. *Details of Exact Low Prandtl Number Boundary-Layer Solutions for Forced and For Free Convection*; No. NASA-MEMO-2-27-59E; NTRS: Washington, DC, USA, 1959.
37. Hossain, M.A.; Takhar, H.S. Radiation effect on mixed convection along a vertical plate with uniform surface temperature. *Heat Mass Transf.* **1996**, *31*, 243–248.
38. Damseh, R.A. Magneto hydrodynamics-mixed convection from radiate vertical isothermal surface embedded in a saturated porous media, *J. Appl. Mech.* **2006**, *73, 54–59*.
39. Zahmatkesh, I. Influence of thermal radiation on free convection inside a porous enclosure. *Emir. J. Eng. Res.* **2007**, *12*, 47–52.
40. Pal, D.; Mondal, H. Radiation effects on combined convection over a vertical flat plate embedded in a porous medium of variable porosity. *Meccanica* **2009**, *44*, 133–144.
41. Mohamed, R.A.; Abo-Dahab, S.M. Influence of chemical reaction and thermal radiation on the heat and mass transfer in MHD micropolar flow over a vertical moving porous plate in a porous medium with heat generation. *Int. J. Therm. Sci* **2009**, *48*, 1800–1813.
42. Bhattacharyya, K.; Mukhopadhyay, S.; Layek, G.C.; Pop, I. Effects of thermal radiation on micropolar fluid flow and heat transfer over a porous shrinking sheet. *Int. J. Heat Mass Transf.* **2012**, *55*, 2945–2952.
43. Pal, D.; Chatterjee, S. MHD mixed convection stagnation-point flow of a micropolar fluid in a porous medium towards a heated stretching sheet with thermal radiation. *Math. Model. Anal.* **2012**, *17*, 498–518.
44. Moradi, A.; Ahmadikia, H.; Hayat, T.; Alsaedi, A. On mixed convection–radiation interaction about an inclined plate through a porous medium. *Int. J. Therm. Sci.* **2013**, *64*, 129–136.
45. Sheikholeslami, M.; Gorji-Bandpy, M.; Ganji, D.D. Numerical investigation of MHD effects on Al2O3–water nanofluid flow and heat transfer in a semi-annulus enclosure using LBM. *Energy* **2013**, *60*, 501–510.
46. Hussain, M.; Ashraf, M.; Nadeem, S.; Khan, M. Radiation effects on the thermal boundary layer flow of a micropolar fluid towards a permeable stretching sheet. *J. Frankl. Inst.* **2013**, *350*, 194–210.
47. Mukhopadhyay, S. Slip effects on MHD boundary layer flow over an exponentially stretching sheet with suction/blowing and thermal radiation. *Ain Shams Eng. J.* **2013**, *4*, 485–491.
48. Hayat, T.; Shehzad, S.A.; Qasim, M.; Asghar, S.; Alsaedi, A. Thermally stratified radiative flow of third grade fluid over a stretching surface. *J. Thermopphys. Heat Transf.* **2014**, *28*, 155–161.
49. Prakash, D.; Muthtamilselvan, M. Effect of radiation on transient MHD flow of micropolar fluid between porous vertical channel with boundary conditions of the third kind. *Ain Shams Eng. J.* **2014**, *5*, 1277–1286.
50. Uddin, Z.; Kumar, M.; Harmand, S. Influence of thermal radiation and heat generation/absorption on MHD heat transfer flow of a micropolar fluid past a wedge considering hall and ion slip currents. *Therm. Sci.* **2014**, *18* (Suppl. 2), 489–502.
51. Cortell, R.A. Nnumerical tackling on Sakiadis flow with thermal radiation. *Chin. Phys. Lett.* **2008**, *25*, 1340.
52. Siegel, R.; Howell, J.R. *Thermal Radiation: Heat Transfer*; 3rd ed.; Hemisphere: Washington, DC, USA, 1992.
53. Sparrow, E.M.; Cess, R.D. *Radiation Heat Transfer*; Hemisphere: Washington, DC, USA, 1978.